Intrinsic dynamics shape responses to external stimulation in the human brain

Maximilian Nentwich[1], Stephan Bickel[1,2,3], Lucas C. Parra[4]

[1] The Feinstein Institutes for Medical Research, Northwell Health, Manhasset, NY, USA; [2] Departments of Neurology and Neurosurgery, Zucker School of Medicine at Hofstra/Northwell, Hempstead, NY, USA; [3] Center for Biomedical Imaging and Neuromodulation, Nathan Kline Institute, Orangeburg, NY, USA; [4] Department of Biomedical Engineering, The City College of New York, New York, NY, USA

Abstract

When ongoing sensory stimulation reaches the brain, the resulting neural activity reverberates in its recurrent neural networks. How this intrinsic dynamic affects sensory responses is not well understood. To separate the immediate effect of the stimulus from the recurrent brain dynamic we used a new vector-autoregressive model with external input (VARX). Applying this analysis to intracranial recordings in humans, we find that the recurrent connectivity observed during rest is unaltered when humans are watching movies. The recurrent dynamic enhances and prolongs the responses of the brain to scene cuts, fixation onsets, and sound envelope. If one fails to account for these external inputs, then spurious connections appear in the “functional connectivity”. The model reproduces the prominent observation that an external stimulus can reduce intrinsic noise. The model also reveals that sensory areas have mostly outward connections, whereas higher-order brain areas have mostly incoming connections. By combining the concepts of “functional connectivity” and “encoding models” we introduce an analytical approach capable of revealing interactions between external stimulation and internal dynamics that are not apparent when analyzing these concepts in isolation.

Introduction

The brain is highly interconnected between and within brain areas. Strikingly, most models of brain activity in response to external natural stimuli do not take the recurrent architecture of brain networks into account. "Encoding" models often rely on simple input/output relationships such as general linear models in fMRI (Friston et al., 1995), or temporal response functions in EEG/MEG (Lalor and Foxe, 2010). Interaction between brain areas is captured instead during rest, often just as instantaneous linear correlations that are referred to as "functional connectivity" (Greicius et al., 2003). By taking temporal precedence into account with linear predictive models the "Granger-causality" formalism can establish directed "connectivity" in recurrent models (Friston et al., 2013; Haufe et al., 2013; Pellegrini et al., 2023; Seth et al., 2015; Sheikhattar et al., 2018; Soleimani et al., 2022).

The concept of functional connectivity was first developed to analyze neural activity during rest, where there are no obvious external signals to associate with brain activity. But it is now also often used in the presence of a task or continuous natural stimulus such as watching movies (Betti et al., 2013; Geerligs et al., 2015; Mennes et al., 2013; Vanderwal et al., 2017). A general observation of these studies is that a portion of the functional connectivity is preserved between rest and task conditions, while some aspects are altered by the task (Cole et al., 2014; Mennes et al., 2013). This should be no surprise, given that an external stimulus can drive multiple brain areas and thus induce correlations between these areas (Cole et al., 2019). Removing such “spurious” correlations by controlling for a common cause is standard practice in statistical modeling and causal inference (Pearl, 2013). However, stimulus-induced correlations are often ignored when analyzing the correlation structure of neural signals, with the notable exception of “dynamic causal modeling” (Friston et al., 2003).

We will ask here whether, after removing such spurious correlations, the intrinsic dynamic itself is altered by a perceptual task. Attempts to do this come from work on response variability. For instance, fMRI shows that variability across trials in motor cortex is due to an intrinsic “noise” which is linearly superimposed on a more reliable response to a simple motor action (Fox et al., 2006). Stimulus-response variability in the visual cortex has been attributed to variability of ongoing dynamic (Arieli et al., 1996). Some studies of electrical recordings from the visual cortex show that correlations of spiking activity between locations are largely unaffected by visual stimulation (Fiser et al., 2004). Yet, other studies show that visual input affects local correlation in the visual cortex (Ito et al., 2020; Nauhaus et al., 2009).

The technical challenge when addressing these questions is to separate the direct effect of the stimulus from the intrinsic recurrent dynamic. Here we propose to separate these effects by modeling them simultaneously with the simplest possible model, namely, a linear model that captures intrinsic connectivity and responses to extrinsic input. A mode of that nature is the vector-autoregressive model with external input (VARX). This model is well established in the field of linear systems (Ljung, 1999) and econometrics (Hamilton, 2020), where it is used to capture intrinsic dynamics in the presence of an external input. The VARX model is an extension of the VAR model that is routinely used to establish "Granger-causality". An advantage of the formalism is that it provides a measure of statistical significance and directionality of effects for the intrinsic dynamic and the external input with a single model (Parra et al., 2024).

While linear systems are an inadequate model of neuronal dynamics, they remain an important tool to understand neural representations because of their conceptual simplicity. They are routinely used for event-related fMRI analysis but also for “encoding models” to link non-linear features of continuous stimuli to neural responses, such as responses to video in fMRI (Naselaris et al., 2011), to speech in EEG (Di Liberto et al., 2015) or to audio in intracranial EEG (Holdgraf et al., 2017). They have been used even to understand encoding in deep-neural network models (Li et al., 2023). Here we use a classic linear model to combine two canonical concepts which have thus far remained separated, namely, that of “encoding models” (Naselaris et al., 2011) and “functional connectivity” (Friston et al., 2013). We do this for the first time including the Granger formalism. We will use this to analyze whole-brain, intracranial EEG

in human subjects at rest, and while they watch videos. Our main finding is that the recurrent dynamic observed during rest is only minimally altered by this video task. Instead, the response of the brain to the naturalistic stimulus appears to be substantially shaped by the endogenous dynamic of the brain.

Methods

The vector-autoregressive model with external input (VARX) falls within a group of well-established linear models (see Table 1). Prominent examples in this group are the generalized linear model (GLM) and dynamic causal model (DCM). While these models have been extensively used for neural signal analysis, the VARX model has not. We start therefore with a brief introduction. For more details please refer to (Parra et al., 2024)

VARX model:

The VARX model explains a time-varying vectorial signal $\mathbf{y}(t)$ as the result of an intrinsic autoregressive feedback driven by an innovation process $\mathbf{e}(t)$ and an extrinsic[1] input $\mathbf{x}(t)$:

$$\mathbf{y}(t) = \mathbf{A} * \mathbf{y}(t-1) + \mathbf{B} * \mathbf{x}(t) + \mathbf{e}(t)$$

$\mathbf{A}*$ and $\mathbf{B}*$ represent convolutions with appropriately sized matrices of causal filters with lengths n_a and n_b respectively. $\mathbf{A}$ and $\mathbf{B}$ are unknown and are to be estimated from the observed history of $\mathbf{x}(t)$ and $\mathbf{y}(t)$, assuming minimal contribution from an unobserved normal i.i.d. innovation process $\mathbf{e}(t)$. The role of each of these terms for brain activity is explained in Fig. 1.

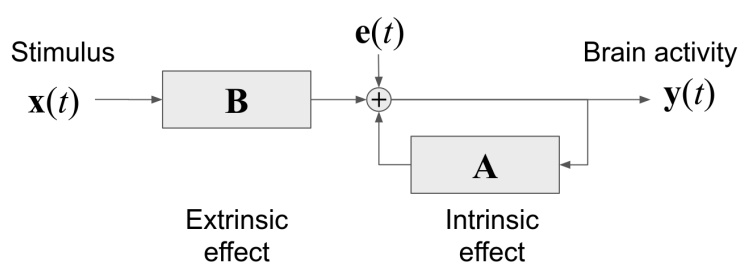

Figure 1: VARX model of the brain: $\mathbf{y}(t)$ represents observable neural activity in different brain areas, $\mathbf{x}(t)$ are observable features of a continuous sensory stimulus, $\mathbf{A}$ represent the recurrent connections within and between brain areas (intrinsic effect), and $\mathbf{B}$ captures the transduction of the sensory stimuli into neural activity and transmission to different brain areas

[1] We adopt here the terminology of “Intrinsic” and “extrinsic” as it is commonly used in neuroscience and psychology. In system modeling and econometrics, where the VARX model is prevalent, the more common terminology is “endogenous” and “exogenous”, meaning effectively the same thing.

(extrinsic effect). The diagonal term in $\mathbf{A}$ captures recurrent feedback within a brain area. Finally, $\mathbf{e}(t)$ is unobserved intrinsic “random” brain activity.

Filter matrices $\mathbf{A}$ and $\mathbf{B}$ can be estimated efficiently with ordinary least squares (OLS) by minimizing the mean squared innovation,

$$\boldsymbol{\sigma}^2 = 1/T \sum_{t=1}^{T} \mathbf{e}(t)^2 .$$

Granger analysis

The innovation is also the prediction error, for predicting $\mathbf{y}(t)$ from the past $\mathbf{y}(t-1)$ and input $\mathbf{x}(t)$. In the Granger formalism the prediction error is calculated with all predictors included (full model, $\boldsymbol{\sigma}_f$) or with individual dimension in $\mathbf{y}(t-1)$ or $\mathbf{x}(t)$ omitted (reduced models, $\boldsymbol{\sigma}_r$) (Granger, 1969). To quantify the "effect" of the specific dimension one can take the ratio of these errors (Geweke, 1982) leading to the test statistic D known as the "deviance". For large T, the deviance follows the Chi-square distribution with cumulative density F, from which one can compute a p-value:

$$\begin{aligned} D &= T \log(\boldsymbol{\sigma}_r^2 / \boldsymbol{\sigma}_f^2) \\ p &= 1 - F(D, T) \\ R^2 &= 1 - \exp(-D/T) \end{aligned}$$

The p-value quantifies the probability that a specific connection in $\mathbf{A}$ or $\mathbf{B}$ is zero. The "generalized" R^2 (Magee, 1990) serves as a measure of effect size, or strength of each connection (D, p and R can be computed for each connection in matrix $\mathbf{A}$ or $\mathbf{B}$).

Overall system response

The overall brain response to the stimulus for the VARX model is given by the system impulse response (written here in the z-domain of Fourier domain):

$$\mathbf{H} = (1 - \mathbf{A})^{-1} \mathbf{B}.$$

What we see here is that the system response $\mathbf{H}$ is factorized into an autoregressive (AR) filter $\mathbf{A}$ and a moving average (MA) filter $\mathbf{B}$. When modeled as a single MA filter in the neuroscience community the total system response has been called the “multivariate Temporal Response Function” (mTRF) (Crosse et al., 2016). We found that the VARX estimate of $\mathbf{H}$ is nearly identical to the estimated mTRF (see Fig. 4 in (Parra et al., 2024). In other words, $\mathbf{B}$ and $\mathbf{A}$ are a valid factorization of the mTRF into immediate and recurrent effects.

Relation to common neural signal models

The VARX model fits naturally into the existing family of models used for neural signals analysis (Table 1). While they differ in the formulation and statistical assumptions, their defining equations has a similar general form with the following attributes:

Table 1: Models commonly used in neural signal analysis

Model	Intrinsic effect $\mathbf{A}$	Extrinsic effect $\mathbf{B}$	Interact	Delay n_a, n_b	Estimation speed	Reference, with code where available
GLM	no	yes	no	=1	medium	(Friston et al., 1994), SPM, FSL
DCM	yes	yes	yes[2]	=1[3]	slow	(Friston et al., 2003), no code
VAR	yes	no	no	>1	fast/slow	(Barnett and Seth, 2014)
mTRF	no	yes	no	>1	fast	(Crosse et al., 2016)
VARX	yes	yes	no[4]	>1	fast	(Parra et al., 2024)

An important simplifying assumption for the mTRF, VAR, and VARX models is that $\boldsymbol{y}(t)$ is observable with additive normal distributed innovation. As a result, parameter estimation can use OLS, which is fast to compute. In contrast, GLM, DCM, and some variants of VAR models assume that $\boldsymbol{y}(t)$ is not directly observable, and needs to be estimated in addition to the unknown parameters $\mathbf{A}$ or $\mathbf{B}$. The same is true for the basic output error model in linear systems theory (Ljung, 1999). This requires slower iterative algorithms, such as expectation maximization. As a result, these models are often limited to small networks[5] of a few nodes to test specific alternative hypotheses (Penny et al., 2004). In contrast, here we will analyze 100-200 channels per subject to draw general conclusions about overall brain organization.

Validation of connectivity estimate on whole-brain neural mass model

To validate the interpretation that $\mathbf{A}$ is a model of "connectivity", we simulated neural activity for a whole-brain neural mass model (Cakan et al., 2023). We used the default model of the neurolib python library ("ALNModel"), which is a mean-field approximation of adaptive exponential integrate-and-fire neurons. This model can generate simulated mean firing rates in 80 brain areas based on connectivity and delay matrices determined with diffusion tensor imaging (DTI). We used 5 min of "resting state" activity (no added stimulus, simulated at 0.1ms resolution, subsequently downsampled to 100Hz). The true connectivity matrix from DTI (Fig. 2A) appears to be similar to the effect size estimate R for the recurrent connections $\mathbf{A}$ in the VARX model with no input (Fig. 1B). Following (Honey et al., 2009) we compare the two as a

---

[2] "Interact" refers to an additional bilinear interaction term of the form $\boldsymbol{x}\,\boldsymbol{C}\,\boldsymbol{y}$ that allows for a modulation of intrinsic effect by the external input.
[3] The DCM is defined in terms of the first derivative of $\boldsymbol{y}(t)$, which in discret time is the same as n_a=1.
[4] It is straightforward to add an interaction term to the VARX model and maintain fast OLS estimation.
[5] The original DCM proposed for fMRI included an added complication of modeling the hemodynamic response, which amounts to adding a temporal filter to each output node and prior to adding observation noise.

scatter plot (Fig. 2C) and observed a Spearman correlation of 0.69. For comparison, we also used the sparse inverse covariance method to recover structural connectivity from functional connectivity. This method is more sensitive than others in detecting network connections (Smith et al., 2011) and uses the graphical lasso algorithm (Chen, 2023). The resulting connectivity estimate (Fig. 1D) only achieves a Spearman correlation of 0.52. We note that the structural connectivity here from DTI is largely symmetric. When enhancing the asymmetry the VARX model is not as accurate, but correctly recovers the direction of the asymmetry (Fig. S9).

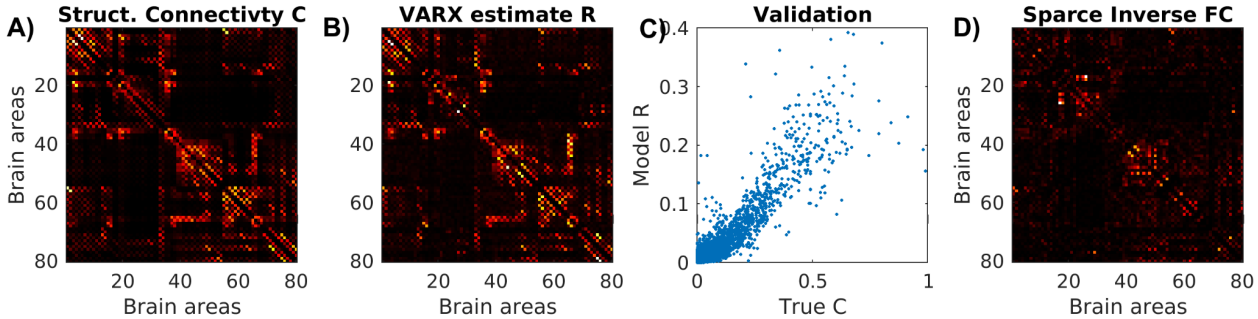

Figure 2: Connectivity of stimulated neural mass model of the whole brain and estimated VARX model. A) True structural connectivity used to simulate neural activity using a neural mass model with the neurolib python toolbox. Connectivity is based on DTI data between 80 brain areas (called Cmat in neurolib). Here showing the square root of the “Cmat" matrix for better visibility of small connectivity values. B) Effect size estimate **R** for the **A** matrix of the VARX model on the simulated data. C) Comparison of true and VARX estimate of connectivity. D) Absolute value of the sparse inverse functional connectivity (estimated using graphical lasso (Friedman et al., 2008)).

Dataset and Methods

We analyzed intracranial EEG and simultaneous eye-tracking data recorded from patients (N=21, mean age 37.81 years, age range 19-58 years, 9 female, Table S1). Three patients underwent two implantations and recordings at different times resulting in a total of 24 recording sessions with a total of 4,962 recording channels. Patients were at rest, or were watching video clips. The video clips included animations with speech (‘Despicable Me’, two different clips, 10 min each, in English and Hungarian), an animated short film with a mostly visual narrative and music, shown twice (‘The Present’, 4.3 min), and three clips of documentaries of macaques (‘Monkey’, 5 min each, without sound) (Nentwich et al., 2020). In addition to the movies from the previous analysis, we included a movie clip of abstract animations (‘Inscapes’, 10 min) (Vanderwal et al., 2015), and an eyes-open resting state with maintained fixation (‘Resting state’, 5 min). In total, we recorded up to 59.3 minutes of data for each patient (Table S1).

Neural signals are preprocessed as previously described to reduce noise (Nentwich et al., 2023). We re-reference signals in a bipolar montage to ensure analysis of local activity. We analyze local field potentials (LFPs) and broadband high-frequency activity (BHA) power. BHA is the power of the signal bandpass filtered between 70-150Hz. We perform analysis on both signals after downsampling to 60Hz.

We extract three features of the movies that serve as external inputs for the VARX model: fixation onset, film cuts and sound envelope. Fixation onset and film cuts are defined as previously described (Nentwich et al., 2023). Sound envelope is computed as the absolute value of the Hilbert transform of the sound from the movie files. The envelope is downsampled to 60 Hz. All videos and resting state include fixations. The video 'Inscapes' and resting state do not include film cuts as external input. The 'Monkey' video clips and resting state do not include the sound envelope as input features. When a feature is not available it is replaced with a vector of Gaussian noise. When comparing models with different features we always keep the number of input variables consistent between models to avoid a bias by the number of free parameters. Features that are not considered in the analysis are shuffled in time by a circular shift by half the duration of the signals.

The VARX models were fit to data with the matlab version of the code at (Parra et al., 2024). For all analyses we use filters of 600 ms length for inputs (n_b=36 samples for VARX models, L=36 samples for mTRFmodels). Delays for connections between channels are set to 100ms (n_a=10 samples) for LFP signals, and 50ms (n_a=5 samples) for faster BHA signals. The regularization parameter was set to λ=0.3.

Connectivity plots are created with nilearn's plot_connectome() function (Fig. 4) (Chamma et al., 2024). We plot connections with an R value above 0.05. Surface plots of T1w/T2w ratios and directionality of connections are created using the field-echos repository (Gao et al., 2020a, 2020b). T1wT2w maps (Glasser et al., 2016) are obtained from the neuromaps repository (Markello et al., 2024, 2022), and transformed to the freesurfer surface using the fslr_to_fsaverage() function (Robinson et al., 2018, 2014).

All analysis code is available on github (https://github.com/MaxNentwich/varx_demo). Figure data will be available on OSF.

Results

Extrinsic input causes spurious connectivity

To determine the effect of the extrinsic inputs on connectivity estimates we either fit a VARX model or a VAR model (i.e. a VARX model with no external input). We analyze LFP data on all available recordings, movies and resting state for all N=24 recording sessions. As extrinsic inputs we included film cuts, fixation onset, and sound envelope. VAR models contain the same external inputs as the VARX model, but they are not aligned in time. The VAR and VARX models have a similar connectivity structure (Fig. 3A and 3B). However, they vary systematically in the number of significant recurrent connections $\mathbf{A}$ (those with p<.0001, Fig. 3D), which drops when adding inputs (t(23)=-4.8, p<0.0001). The effect sizes R are also significantly decreases in the VARX model (Fig. 3E, t(23)=-4.8, p<0.0001). Therefore, accounting for the external input removes spurious "connections". We also analyze how much each of these features contributed to this effect (Fig. 3F). Evidently all features contributed to some degree, and likely other

features of the movie may further reduce stimulus-induced connections. Out of the three features considered, models including fixations and cuts decrease effect size more than models with sound envelope (fixations vs. sound, t(23)=-2.83, p=0.0093; cuts vs. sound: t(23)=-3.51, p=0.0019; uncorrected). The model including the combination of all three features has a smaller effect size than models with any individual feature (all vs. fixations, t(23)=-8.24, p<.0001; all vs. cuts: t(23)=-3.91, p<.001; all vs. sound t(23)=-4.35, p<.001; uncorrected). Thus, more input features further reduce the strength of spurious correlations. These results are also reflected in the analysis of BHA signals (Fig. S1).

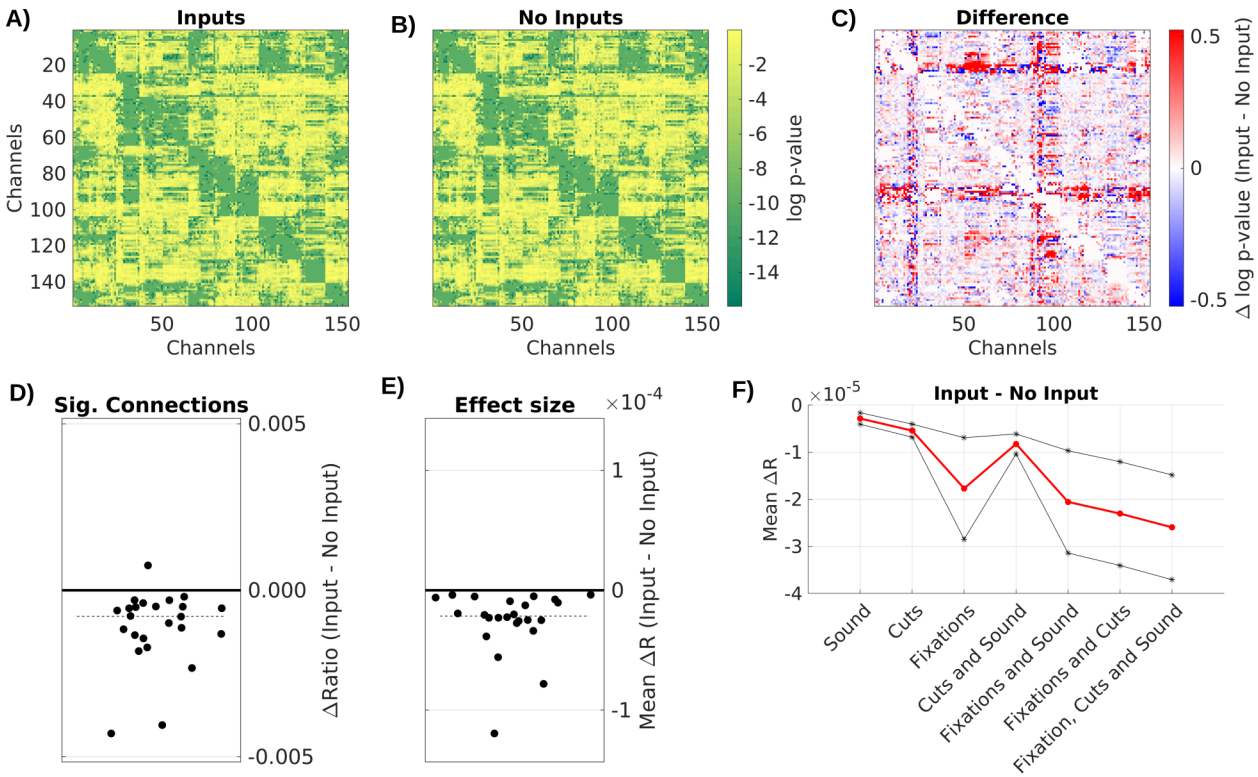

Figure 3: Spurious recurrent connectivity in $\mathbf{A}$ is removed when modeling the effect of exogenous input with $\mathbf{B}$. Comparison of VARX model with and without inputs. A) p-values for each connection in $\mathbf{A}$ for VARX model with inputs on one subject (Pat_1); B) for VARX model without inputs; C) difference. Both models are fit to the same data. D) Difference of fraction of significant recurrent connections between VARX models with and without inputs. E) Mean difference in R over all electrodes between VARX models with and without inputs. Each point is a subject. Dashed line is the median across subjects. F) Difference between the VARX models with different combinations of inputs and VARX model without inputs. Red line shows mean across patients, black lines the 95% confidence interval. Negative values indicate a drop in connectivity strength when exogenous input is accounted for.

Recurrent connectivity unchanged during movies and rest

Next we compared intrinsic connectivity between movie watching and rest (Fig. 4A-D). In the rest condition subjects have a fixation cross, but still move their eyes. We therefore use a VARX model including fixation onset as extrinsic variable in both cases. Movies include film cuts and the sound envelope as external inputs. To control for the number of free parameters, we include copies of the film cut and sound envelope features from the movies to the resting state model. Two patients did not complete both movie watching and resting state and are not included in this analysis (Pat_5 & Pat_16). Remarkably, the number of significant recurrent connections is unchanged between movie watching and rest (Fig. 4C, student t-test, t(21)=-1.40, p=0.18), as is the effect size (Fig. 4D, student t-test, t(21)=-1.70, p=0.10). One caveat to this conclusion is that the signal we analyzed was only 5 minutes long for the movie and rest conditions. This might be too short to detect differences. However, even on 5 minutes of data we observe a decrease in R values when including external inputs (Fig S2). We also find that intrinsic connectivity of BHA between movie and rest does not differ (Fig. S3). This suggests that the differences in the intrinsic connectivity between movie and rest, if they exist, are less systematic than the effect of the stimulus.

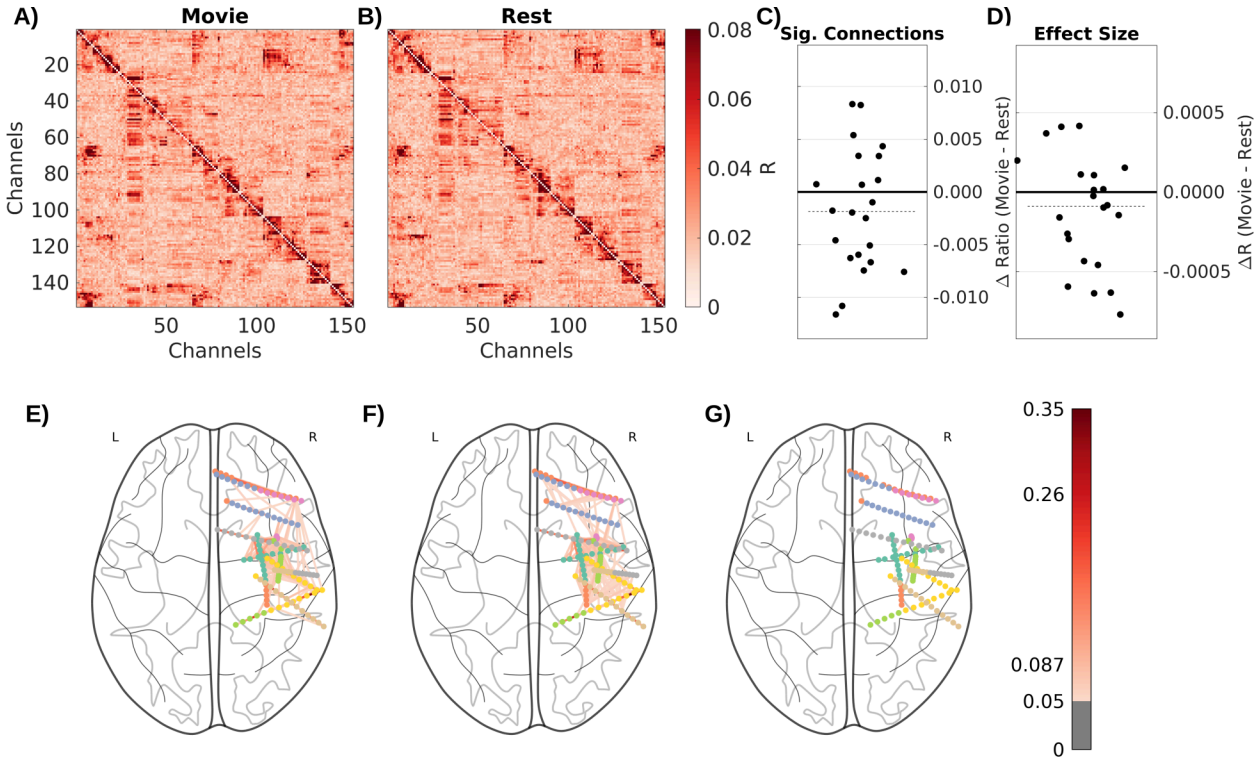

Figure 4: Recurrent connectivity A during movies does not differ from rest. Coefficient of determination R for each connection. A) VARX model of 5 minutes of LFP recordings during movie watching, with sound envelope, fixation onsets and film cuts as input features. B) VARX model during resting fixation with fixation onset as input feature. C) Difference in the number of significant connections (p<.0001) between movie and rest. D) Difference in mean effect size

across all channels between movie and rest. Dots represent subjects, dashed line the median across subjects. Axial view of connections in E) the movie task, F) resting state, and G) the difference between movies and resting state. For plotting purposes connections in the upper triangle are plotted and asymmetries ignored. Connections with R values below 0.05 are not shown.

Recurrent dynamic enhances and prolongs stimulus responses

We also compared the total system response $\mathbf{H}$, which includes the immediate effect of $\mathbf{B}$, as well as the recurrent effects of $\mathbf{A}$ (Fig. 5). We analyze the VARX model shown in Fig. 3B and compare the effect of inputs $\mathbf{B}$ to the filters from TRF models $\mathbf{H}$. Both models include fixation onset, and sound envelope as external inputs. We compare the power and length of filters from both models. Power is computed as the average of the instantaneous power, i.e. the square of the weight at each delay of the filters. Length is computed as the 'peak widths' argument of Matlab's findpeaks() function. We compare responses in channels with significant effects of $\mathbf{B}$ (FDR correction, α=0.05). We see that the total response is significantly stronger (Fig. 5C, t(23)=-6.42 p<.0001) and longer than the immediate effect of the input (Fig. 5D, t(23)=-5.63, p<.0001). The same effect is observed in BHA responses (Fig. S5).

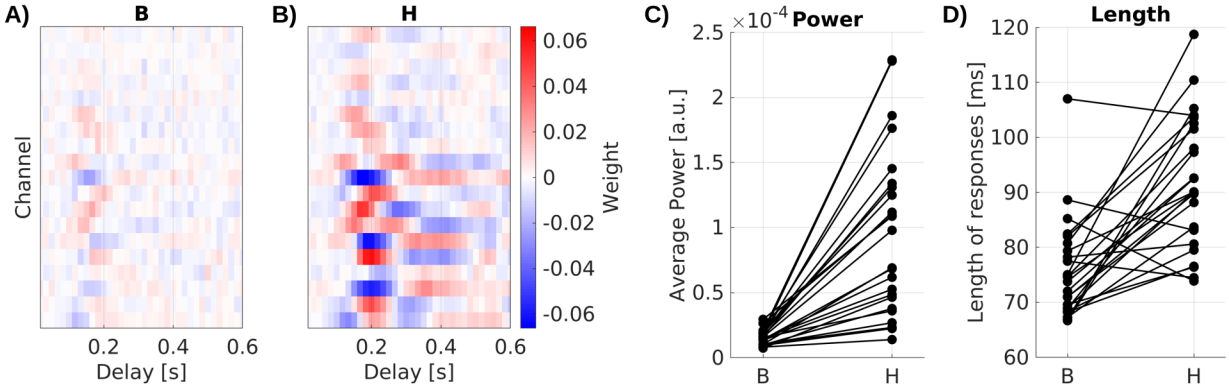

Figure 5: Impulse response models. A) Immediate responses $\mathbf{B}$ to auditory envelope are weaker and shorter than B) the overall system response $\mathbf{H}$. Significant responses for Pat_1. C) Power and D) mean length of responses in significant channels for all patients. Each line is a patient. Responses to fixation onset and film cuts are shown in Figure S4.

Effects are the same for LFP and BHA

We repeated the same analyses of Figures 3-5 with broadband high frequency activity (BHA), which is thought to represent a proxy for neural population firing in the vicinity of an electrode. Generally we find a more sparse recurrent connectivity for BHA as compared to LFP, which is thought to capture dendritic currents (compare Fig. 3-5 with Fig. S1,S3&S5). Regardless of this overall difference, we find the same results hold when analyzing BHA. Namely, taking the extrinsic input into account results removed spurious "connections" (Fig. S1); the resulting model of the recurrent dynamic is indistinguishable between watching movies and rest (Fig. S3);

and responses to the stimulus are stronger and more prolonged when separately modeling the effect of recurrent connectivity (Fig. S5).

Intrinsic noise is reduced by external stimulus

So far we have discussed the mean response captured by $\mathbf{B}$ and the recurrent activity mediated by $\mathbf{A}$. We now want to analyze whether the external input modulates the variability of the internal dynamic. As a metric of internal variability we measured here the power of the intrinsic innovation process $\mathbf{e}(t)$. When the model better captures intrinsic and extrinsic dynamics $\mathbf{e}(t)$ is expected to decrease. For the LFP signal we see a drop in power during movies as compared to rest, for both the original signal $\mathbf{y}(t)$ (Fig. S6A) and the model's innovation process $\mathbf{e}(t)$ (Fig. S6B). Notable is the stronger oscillatory activity during rest (Fig. S6A), which we observed in most patients. When analyzing BHA, we find no difference in power of the innovation process between movie and rest, but we do find a drop in power relative to the overall BHA signals for some channels (Fig. 6B). These channels seem to coincide with channels that responded to the external stimuli, i.e. channels with a significant effect in $\mathbf{B}$ (Fig. 6A). If we take for each subject the median relative power for responsive channels (median among those with $p<0.0001$), then we find that relative power drops for nearly all subjects (Fig 6D, Wilcoxon rank sum test, $p=2.6e-06$, $N=21$). 21 patients with both movie and resting state data and with channels with significant responses to external input are included in this analysis. The motivation for analyzing only responsive channels comes from a simple gain adaptation (Fig. S8). Gain adaptation keeps the power of $\mathbf{y}(t)$ constant, so that the extra power injected by the stimulus in responsive channels indirectly reduces the relative power of the innovation process. This effect is specific to channels that receive an external input (Figl. S8C) and absent in a linear system without gain adaptation (Fig. S8D). To demonstrate that this simple gain adaptation can explain the noise quenching in the neural data, we simulated data with the gain adaptation model (Fig. 6C) using parameters estimated for the example subject of Fig. 6A/B.

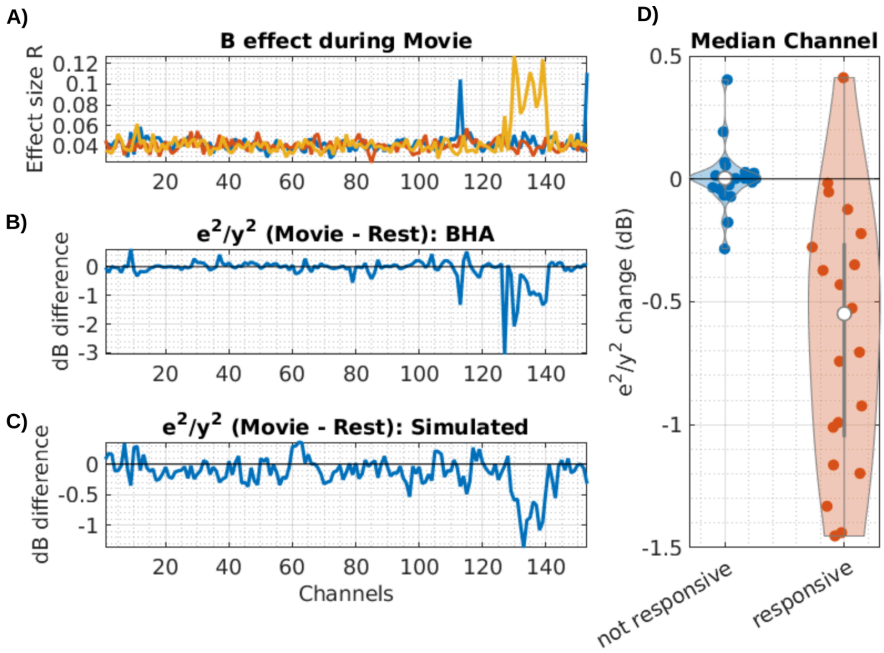

Figure 6: For BHA, relative power of innovation vs signal drops during movies as compared to rest in responsive channels. A) Effect size R for B in all channels to 3 inputs (scene cuts, fixation onset, sound envelope). In this example 15 electrodes had significant responses to one of the three inputs (Bonferroni corrected at p<0.01). B) Change in relative power of innovation (dB(innovation power / signal power), then subtracting movie - rest). C) Change in relative power of innovation in a simulation of a VARX model with gain adaptation. Here we are using the A and B filters that were estimated on BHA on the example from panel A and B. D) Median of power ratio change across all subjects, contrasting responsive vs non-responsive channels.

Direction of connectivity differs with cortical hierarchy

Finally, we measured the directionality of the recurrent connections by analyzing the structure of the resulting matrices R of all subjects. Columns in R represent outgoing connections, while rows are incoming connections. Therefore, the mean difference of $R - R^{\top}$ along a column (Fig. 7A) has positive values if a node has overall stronger outgoing connections, and negative values if it has stronger incoming connections. We measured this directionality for each channel across all subjects and average across channels within parcels of the Desikan-Killiany atlas (N=35 regions of interest, Fig. 7B) (Desikan et al., 2006). We expected this to co-vary with "cortical hierarchy". To test this, we compared this asymmetry metric with the T1w/T2w ratio, which captures gray matter myelination and is used as an indirect measure of cortical hierarchy (Gao et al., 2020a; Wang, 2020). We average T1w/T2w ratio in the same parcels of the Desikan-Killiany atlas (Fig. 7B). Cortical areas showing more outgoing connections ($R - R^{\top}$ > 0) have lower T1w/T2w ratio, which are located higher on the cortical hierarchy (Pearson's r = 0.39, p = 0.023, Fig. 7C). BHA analysis shows the same correlation (Fig. S7).

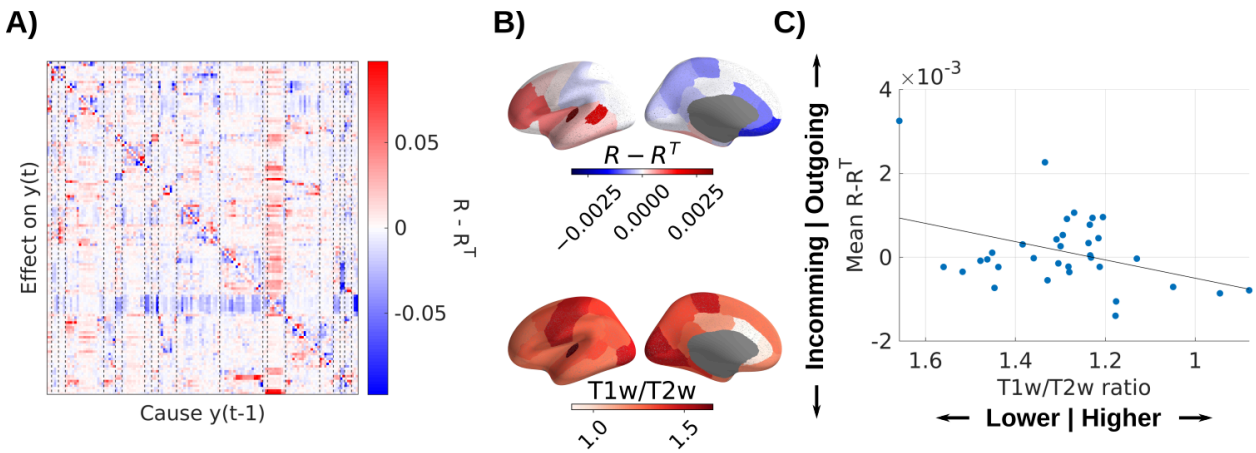

Figure 7: Recurrent connectivity is directed from sensory to higher-order areas. A) Difference of $R - R^\top$ showing asymmetric directed effects. Dashed lines indicate regions of interest in the Desikan-Killiany atlas. B) Mean directionality across patients and T1w/T2w ratio are averaged in parcels of the Desikan-Killiany atlas. C) Mean directionality is correlated with cortical hierarchy, estimated with the T1w/T2w hierarchy.

Discussion

Our results suggest that intrinsic dynamics are not substantially altered during watching movies as compared to rest. Instead, the external stimulus reverberates in the recurrent network with the same dynamic as during rest, resulting in an apparent change of “functional connectivity”.

Intrinsic dynamic versus response to extrinsic input

The previous literature does not clearly distinguish between intrinsic connectivity and extrinsic effects. As a result, similarities and differences between rest and task conditions reported previously, do not draw a firm conclusion as to whether “functional connectivity” is preserved, e.g. (Gonzalez-Castillo and Bandettini, 2018). By systematically factoring out the effect of external input we conclude that the intrinsic dynamic is unaltered.

Conventional “encoding” models, such as the TRF models, capture the entire response of the brain to an external stimulus. Here we decompose this into a MA and AR portion. The AR portion inherently captures longer lasting responses because it naturally models infinite impulse responses. One could think of the recurrent dynamic applying additional filtering to the initial impulse response $\boldsymbol{B}$. The important observation is that this internal dynamic governed by A is identical to that of the resting state. Therefore, an alternative view is that the brian has a static internal dynamic, and that the initial responses $\boldsymbol{B}$ shape the input to be processed by the existing internal dynamical system. This interpretation is consistent with the view of “the brain from the inside out” advocated by György Buzsáki (Buzsaki, 2019). In this view, learning of a representation consists in learning a mapping of the external stimulus to an existing intrinsic dynamic of the brain.

Reduction of noise in the intrinsic activity due to stimulus

We also analyzed variability of the intrinsic activity by analyzing the power of the innovation process. For BHA, which is thought to predominantly capture neuronal firing, we found that the intrinsic innovation process drops in response to a stimulus. Specifically, there is less relative power in the noise for channels that are responsive to the stimulus. This is consistent with the notion that response variability is due to variability of intrinsic activity (Arieli et al., 1996) which is found to decrease across the brian with the onset of an external stimulus (Churchland et al., 2010). Noise quenching has been associated with increased attention (Arazi et al., 2019) and improved visual discrimination performance (Arazi et al., 2017). The effect we found here can be explained by a VARX model with the addition of a divisive gain adaptation mechanism that keeps the total power of brain activity constant. When the input injects additional power, this nonlinear gain adaptation implicitly reduces the contribution of the innovation to the total power.

We also observed an overall drop in LFP power during movie watching. This phenomenon was strongest in oscillatory bands that differed across subjects. In scalp EEG noise quenching was associated with a similar overall drop in power with the stimulus (Arazi et al., 2019). This "quenching" of neural variability was also found to reduce correlation between brian areas for fMRI and neural spiking (Ito et al., 2020), most closely related to BHA. This is at variance with our finding that intrinsic connectivity in BHA does not change significantly between movie and rest. However, we can not rule out such differences on longer recordings.

Alternative approaches

The traditional VAR model has been used extensively in neuroscience to establish directed "Granger causal" connections (Barnett and Seth, 2014). This approach has been very fruitful and found numerous extensions, e.g. (Sheikhattar et al., 2018; Soleimani et al., 2022). However, these model implementations do not specifically account for an external input.

A few methods have attempted to model the effect of external input on functional connectivity during task conditions, mostly in the analysis of fMRI. One approach is to first model the task evoked activations, equivalent to estimating $\boldsymbol{B}$ alone, and then compute the conventional "functional connectivity", i.e. the correlation matrix, on the residuals $\boldsymbol{e}(t)$ (Fair et al., 2007). Others suggested to estimate $\boldsymbol{B}$ in multiple time windows and then estimate a "task related functional connectivity" by correlating the multiple $\boldsymbol{B}$ over time windows (Rissman et al., 2004). It is not clear that these ad hoc methods systematically separates intrinsic from extrinsic factors.

A more principled modeling approach is "dynamic causal modeling" (DCM) (Friston et al., 2003) and extensions thereof (Ryali et al., 2011). Like in the VARX model, DCM includes intrinsic and extrinsic effects $\boldsymbol{A}$ and $\boldsymbol{B}$. However, the modeling is limited to first-order dynamics (i.e. n_a=n_a=1). Instead, the DCM includes a multiplicative interaction of extrinsic input $\boldsymbol{x}(t)$ on the connectivity $\boldsymbol{A}$, which does not exist in the VARX model. This interaction has been used to explicitly model a change in intrinsic connectivity with task conditions. Here we found that this is not necessary for intracranial EEG. A practical advantage of the VARX model is the assumption that the neural activity is directly observed. Instead, many existing models assume an error in the observations,

which triggers computationally intensive estimation algorithms, typically the EM algorithm. The same is true for the basic output error model in linear systems theory (Ljung, 1999). As a result, these models are often limited to small networks[6] to test specific alternative hypotheses (Penny et al., 2004). In contrast, here we have analyzed on each subject 100-200 channels available across the brain, and have drawn more general conclusions about brain activity.

Caveats:

The lack of a meaningful difference in recurrent connectivity between stimulus and rest should be interpreted with care. As usual, lack of evidence is not evidence for a lack of an effect. Indeed, we saw no change in the number of recurrent connections with the movie for LFPs or BHA, although there was a trend towards reduced connectivity strength. It is possible that regressing out a richer stimulus characterization would have removed additional stimulus-induced spurious correlations, only enhancing this small difference between movie and rest. Higher recurrent connectivity in the LFP during rest would be consistent with the more synchronized state we saw in rest, as reflected by larger oscillatory activity.

We find a correlation of DTI structural connectivity used in a model with a VARX estimate of 0.70. That is considered a relatively large value compared to other studies that attempt to recover DTI connectivity from the correlation structure of fMRI activity (Honey et al., 2009). A Caveat is that this was done on a model of firing rate, not fMRI, and we have not explored the parameters of the neural mass model that might affect the results.

We used here fixation onsets as external input, but it should be noted that they are tightly correlated in time with saccade onsets (there is only about a 30 ms jitter between the two, depending on saccade amplitude). Saccades are generated by the brain itself and arguably could also be seen as intrinsic. The same is true for all motor behaviors, most of which cause a corresponding sensory response. Including them as external input is a modeling choice we have made here, but it is important to acknowledge that fixation onsets can therefore have “acausal” components (Nentwich et al., 2023). This could be captured by the VARX Granger formalism by delaying the input relative to the neural activity, which we have not done here.

The correlation between the average incoming and outgoing connections and cortical hierarchy (Figure 7) is not significant when normalizing for the number of electrodes in each region of interest. Regions in the temporal lobe with a large number of electrodes might drive this correlation. A more fine grained analysis in these regions could be the goal of future analysis.

Conclusion

We analyzed whole-brain intracranial recordings in human subjects at rest and while they watched videos. We used a model that separates intrinsic dynamics from extrinsic effects. We

---

[6] The original DCM proposed for fMRI included an added complication of modeling the hemodynamic response, which amounts to adding a temporal filter to each output node and prior to adding observation noise.

found that the recurrent dynamic observed during rest is largely unaltered by the task. Instead, the response of the brain to the stimulus appears to be substantially shaped by its stable endogenous dynamic. The reduction in intrinsic variance observed during an extrinsic stimulus may be the result of neuronal gain adaptation.

Acknowledgements

We would like to thank Chris Honey for advice on the model validation with simulations and related references. We would like to thank Charlie Schroeder for pointing us to the literature on the effect of visual stimulation of intrinsic activity.

References

Arazi, A., Censor, N., Dinstein, I., 2017. Neural Variability Quenching Predicts Individual Perceptual Abilities. J. Neurosci. 37, 97–109. https://doi.org/10.1523/JNEUROSCI.1671-16.2016

Arazi, A., Yeshurun, Y., Dinstein, I., 2019. Neural Variability Is Quenched by Attention. J. Neurosci. 39, 5975–5985. https://doi.org/10.1523/JNEUROSCI.0355-19.2019

Arieli, A., Sterkin, A., Grinvald, A., Aertsen, A., 1996. Dynamics of Ongoing Activity: Explanation of the Large Variability in Evoked Cortical Responses. Science 273, 1868–1871. https://doi.org/10.1126/science.273.5283.1868

Barnett, L., Seth, A.K., 2014. The MVGC multivariate Granger causality toolbox: A new approach to Granger-causal inference. J. Neurosci. Methods 223, 50–68. https://doi.org/10.1016/j.jneumeth.2013.10.018

Betti, V., Della Penna, S., de Pasquale, F., Mantini, D., Marzetti, L., Romani, G.L., Corbetta, M., 2013. Natural Scenes Viewing Alters the Dynamics of Functional Connectivity in the Human Brain. Neuron 79, 782–797. https://doi.org/10.1016/j.neuron.2013.06.022

Buzsaki, G., 2019. The Brain from Inside Out. Oxford University Press.

Cakan, C., Jajcay, N., Obermayer, K., 2023. neurolib: A Simulation Framework for Whole-Brain Neural Mass Modeling. Cogn. Comput. 15, 1132–1152. https://doi.org/10.1007/s12559-021-09931-9

Chamma, A., Frau-Pascual, A., Rothberg, A., Abadie, A., Abraham, A., Gramfort, A., Savio, A., Cionca, A., Thual, A., Kodibagkar, A., Kanaan, A., Pinho, A.L., Idrobo, A.H., Kieslinger, A.-S., Rokem, A., Mensch, A., Vijayan, A., Duran, A., Cipollini, B., Thirion, B., Nguyen, B., Cakan, C., Gorgolewski, C., Markiewicz, C., Horea, C., Gerloff, C., Roßmanith, C., Reininger, C., Lane, C., Sy, C., Delettre, C., Gale, D., Gomez, D., Bzdok, D., Ellis, D.G., Wassermann, D., Pisner, D., Orfanos, D.P., DuPre, E., Dohmatob, E., Larson, E., Edmond, E., Pedregosa, F., Pollet, F., Liem, F., Paugam, F., Varoquaux, G., Hollander, G. de, Kiar, G., Gilmore, G., Lemaitre, G., Wang, H.-T., Aggarwal, H., Abenes, I., Vogel, J., Margeta, J., Grobler, J., Gors, J., Rasero, J., Kossaifi, J., King, J.-R., Dalenberg, J.R., Lefort-Besnard, J., Dockes, J., Chevalier, J.-A., Wiesner, J., Gorrono, J.H.L., Sassenhagen, J., Huguet, J., Teves, J., Huntenburg, J., Peraza, J.A., Daddy, K.R., Sitek, K., Helwegen, K., Wagstyl, K., Shmelkov, K., Chawla, K., CHEN, K., Sasse, L., Estève, L., Tetrel, L., Paz, L., Pietrantoni, M., Perez-Guevara, M., Wegrzyn, M., Goncalves, M., Dugré, M., Ekman, M., Joulot, M., Sitter, M.C., Rahim, M., Zwally, M., Eickenberg, M., Hanke, M., Notter, M., Waskom, M., Wang, M., Torabi, M., Boos, M., Song, M.S., Clarke,

N., Shah, N., Gensollen, N., Krish, N., Warrington, O., Esteban, O., Sadil, P., Bogdan, P., Reiners, P., Sanz-Leon, P., Herholz, P., Gervais, P., Bellec, P., Glaser, P., Quirion, P.-O., Raamana, P.R., Brito, R., Meudec, R., Luke, R., Williamson, R., Guidotti, R., Phlypo, R., Hammonds, R., Gau, R., Patalasingh, S., Hahn, S., Bougacha, S., Johnson, S.B., Jawhar, S., Steinkamp, S., Singh, S., Meisler, S., Pokharel, S., Lan, S., Takerkart, S., Gezici, T., Samanta, T., Salo, T., Bazeille, T., Vanasse, T., Diogo, V., Michel, V., Fritsch, V., Halchenko, Y., Mzayek, Y., Baratz, Z., Nájera, Ó., 2024. nilearn. https://doi.org/10.5281/zenodo.10948303

Chen, X., 2023. xiaohuichen88/Graphical-Lasso.

Churchland, M.M., Yu, B.M., Cunningham, J.P., Sugrue, L.P., Cohen, M.R., Corrado, G.S., Newsome, W.T., Clark, A.M., Hosseini, P., Scott, B.B., Bradley, D.C., Smith, M.A., Kohn, A., Movshon, J.A., Armstrong, K.M., Moore, T., Chang, S.W., Snyder, L.H., Lisberger, S.G., Priebe, N.J., Finn, I.M., Ferster, D., Ryu, S.I., Santhanam, G., Sahani, M., Shenoy, K.V., 2010. Stimulus onset quenches neural variability: a widespread cortical phenomenon. Nat. Neurosci. 13, 369–378. https://doi.org/10.1038/nn.2501

Cole, M.W., Bassett, D.S., Power, J.D., Braver, T.S., Petersen, S.E., 2014. Intrinsic and Task-Evoked Network Architectures of the Human Brain. Neuron 83, 238–251. https://doi.org/10.1016/j.neuron.2014.05.014

Cole, M.W., Ito, T., Schultz, D., Mill, R., Chen, R., Cocuzza, C., 2019. Task activations produce spurious but systematic inflation of task functional connectivity estimates. NeuroImage 189, 1–18. https://doi.org/10.1016/j.neuroimage.2018.12.054

Crosse, M.J., Di Liberto, G.M., Bednar, A., Lalor, E.C., 2016. The Multivariate Temporal Response Function (mTRF) Toolbox: A MATLAB Toolbox for Relating Neural Signals to Continuous Stimuli. Front. Hum. Neurosci. 10. https://doi.org/10.3389/fnhum.2016.00604

Desikan, R.S., Ségonne, F., Fischl, B., Quinn, B.T., Dickerson, B.C., Blacker, D., Buckner, R.L., Dale, A.M., Maguire, R.P., Hyman, B.T., Albert, M.S., Killiany, R.J., 2006. An automated labeling system for subdividing the human cerebral cortex on MRI scans into gyral based regions of interest. NeuroImage 31, 968–980. https://doi.org/10.1016/j.neuroimage.2006.01.021

Di Liberto, G.M., O'Sullivan, J.A., Lalor, E.C., 2015. Low-Frequency Cortical Entrainment to Speech Reflects Phoneme-Level Processing. Curr. Biol. 25, 2457–2465. https://doi.org/10.1016/j.cub.2015.08.030

Fair, D.A., Schlaggar, B.L., Cohen, A.L., Miezin, F.M., Dosenbach, N.U.F., Wenger, K.K., Fox, M.D., Snyder, A.Z., Raichle, M.E., Petersen, S.E., 2007. A method for using blocked and event-related fMRI data to study "resting state" functional connectivity. NeuroImage 35, 396–405. https://doi.org/10.1016/j.neuroimage.2006.11.051

Fiser, J., Chiu, C., Weliky, M., 2004. Small modulation of ongoing cortical dynamics by sensory input during natural vision. Nature 431, 573–578. https://doi.org/10.1038/nature02907

Fox, M.D., Snyder, A.Z., Zacks, J.M., Raichle, M.E., 2006. Coherent spontaneous activity accounts for trial-to-trial variability in human evoked brain responses. Nat. Neurosci. 9, 23–25. https://doi.org/10.1038/nn1616

Friedman, J., Hastie, T., Tibshirani, R., 2008. Sparse inverse covariance estimation with the graphical lasso. Biostatistics 9, 432–441. https://doi.org/10.1093/biostatistics/kxm045

Friston, K., Moran, R., Seth, A.K., 2013. Analysing connectivity with Granger causality and dynamic causal modelling. Curr. Opin. Neurobiol., Macrocircuits 23, 172–178. https://doi.org/10.1016/j.conb.2012.11.010

Friston, K.J., Harrison, L., Penny, W., 2003. Dynamic causal modelling. NeuroImage 19, 1273–1302. https://doi.org/10.1016/S1053-8119(03)00202-7

Friston, K.J., Holmes, A.P., Poline, J.-B., Grasby, P.J., Williams, S.C.R., Frackowiak, R.S.J., Turner, R., 1995. Analysis of fMRI Time-Series Revisited. NeuroImage 2, 45–53. https://doi.org/10.1006/nimg.1995.1007

Friston, K.J., Holmes, A.P., Worsley, K.J., Poline, J. -P., Frith, C.D., Frackowiak, R.S.J., 1994. Statistical parametric maps in functional imaging: A general linear approach. Hum. Brain Mapp. 2, 189–210. https://doi.org/10.1002/hbm.460020402
Gao, R., van den Brink, R.L., Pfeffer, T., Voytek, B., 2020a. Neuronal timescales are functionally dynamic and shaped by cortical microarchitecture. eLife 9, e61277. https://doi.org/10.7554/eLife.61277
Gao, R., Voytek, B., Olayinka, T., 2020b. rdgao/field-echos: post-publication. https://doi.org/10.5281/zenodo.4362645
Geerligs, L., Rubinov, M., Cam-CAN, Henson, R.N., 2015. State and Trait Components of Functional Connectivity: Individual Differences Vary with Mental State. J. Neurosci. 35, 13949–13961. https://doi.org/10.1523/JNEUROSCI.1324-15.2015
Geweke, J., 1982. Measurement of Linear Dependence and Feedback between Multiple Time Series. J. Am. Stat. Assoc. 77, 304–313. https://doi.org/10.1080/01621459.1982.10477803
Glasser, M.F., Coalson, T.S., Robinson, E.C., Hacker, C.D., Harwell, J., Yacoub, E., Ugurbil, K., Andersson, J., Beckmann, C.F., Jenkinson, M., Smith, S.M., Van Essen, D.C., 2016. A multi-modal parcellation of human cerebral cortex. Nature 536, 171–178. https://doi.org/10.1038/nature18933
Gonzalez-Castillo, J., Bandettini, P.A., 2018. Task-based dynamic functional connectivity: Recent findings and open questions. NeuroImage, Brain Connectivity Dynamics 180, 526–533. https://doi.org/10.1016/j.neuroimage.2017.08.006
Granger, C.W.J., 1969. Investigating Causal Relations by Econometric Models and Cross-spectral Methods. Econometrica 37, 424–438. https://doi.org/10.2307/1912791
Greicius, M.D., Krasnow, B., Reiss, A.L., Menon, V., 2003. Functional connectivity in the resting brain: A network analysis of the default mode hypothesis. Proc. Natl. Acad. Sci. 100, 253–258. https://doi.org/10.1073/pnas.0135058100
Hamilton, J.D., 2020. Time Series Analysis. Princeton University Press.
Haufe, S., Nikulin, V.V., Müller, K.-R., Nolte, G., 2013. A critical assessment of connectivity measures for EEG data: A simulation study. NeuroImage 64, 120–133. https://doi.org/10.1016/j.neuroimage.2012.09.036
Holdgraf, C.R., Rieger, J.W., Micheli, C., Martin, S., Knight, R.T., Theunissen, F.E., 2017. Encoding and Decoding Models in Cognitive Electrophysiology. Front. Syst. Neurosci. 11. https://doi.org/10.3389/fnsys.2017.00061
Honey, C.J., Sporns, O., Cammoun, L., Gigandet, X., Thiran, J.P., Meuli, R., Hagmann, P., 2009. Predicting human resting-state functional connectivity from structural connectivity. Proc. Natl. Acad. Sci. 106, 2035–2040. https://doi.org/10.1073/pnas.0811168106
Ito, T., Brincat, S.L., Siegel, M., Mill, R.D., He, B.J., Miller, E.K., Rotstein, H.G., Cole, M.W., 2020. Task-evoked activity quenches neural correlations and variability across cortical areas. PLOS Comput. Biol. 16, e1007983. https://doi.org/10.1371/journal.pcbi.1007983
Lalor, E.C., Foxe, J.J., 2010. Neural responses to uninterrupted natural speech can be extracted with precise temporal resolution. Eur. J. Neurosci. 31, 189–193. https://doi.org/10.1111/j.1460-9568.2009.07055.x
Li, Y., Anumanchipalli, G.K., Mohamed, A., Chen, P., Carney, L.H., Lu, J., Wu, J., Chang, E.F., 2023. Dissecting neural computations in the human auditory pathway using deep neural networks for speech. Nat. Neurosci. 1–13. https://doi.org/10.1038/s41593-023-01468-4
Ljung, L., 1999. System Identification: Theory for the User. Prentice Hall PTR.
Magee, L., 1990. R 2 Measures Based on Wald and Likelihood Ratio Joint Significance Tests. Am. Stat. 44, 250–253. https://doi.org/10.1080/00031305.1990.10475731
Markello, R., Hansen, J., Liu, Z.-Q., Bazinet, V., Shafiei, G., Suarez, L., Mišić, B., 2024. neuromaps: structural and functional interpretation of brain maps. https://doi.org/10.5281/zenodo.10607923

Markello, R.D., Hansen, J.Y., Liu, Z.-Q., Bazinet, V., Shafiei, G., Suárez, L.E., Blostein, N., Seidlitz, J., Baillet, S., Satterthwaite, T.D., Chakravarty, M.M., Raznahan, A., Misic, B., 2022. neuromaps: structural and functional interpretation of brain maps. Nat. Methods 19, 1472–1479. https://doi.org/10.1038/s41592-022-01625-w

Mennes, M., Kelly, C., Colcombe, S., Castellanos, F.X., Milham, M.P., 2013. The Extrinsic and Intrinsic Functional Architectures of the Human Brain Are Not Equivalent. Cereb. Cortex 23, 223–229. https://doi.org/10.1093/cercor/bhs010

Naselaris, T., Kay, K.N., Nishimoto, S., Gallant, J.L., 2011. Encoding and decoding in fMRI. NeuroImage, Multivariate Decoding and Brain Reading 56, 400–410. https://doi.org/10.1016/j.neuroimage.2010.07.073

Nauhaus, I., Busse, L., Carandini, M., Ringach, D.L., 2009. Stimulus contrast modulates functional connectivity in visual cortex. Nat. Neurosci. 12, 70–76. https://doi.org/10.1038/nn.2232

Nentwich, M., Ai, L., Madsen, J., Telesford, Q.K., Haufe, S., Milham, M.P., Parra, L.C., 2020. Functional connectivity of EEG is subject-specific, associated with phenotype, and different from fMRI. NeuroImage 218, 117001. https://doi.org/10.1016/j.neuroimage.2020.117001

Nentwich, M., Leszczynski, M., Russ, B.E., Hirsch, L., Markowitz, N., Sapru, K., Schroeder, C.E., Mehta, A.D., Bickel, S., Parra, L.C., 2023. Semantic novelty modulates neural responses to visual change across the human brain. Nat. Commun. 14, 2910. https://doi.org/10.1038/s41467-023-38576-5

Parra, L.C., Silvan, A., Nentwich, M., Madsen, J., Babadi, B., 2024. VARX Granger Analysis: Modeling, Inference, and Applications.

Pearl, J., 2013. Linear Models: A Useful “Microscope” for Causal Analysis. J. Causal Inference 1, 155–170. https://doi.org/10.1515/jci-2013-0003

Pellegrini, F., Delorme, A., Nikulin, V., Haufe, S., 2023. Identifying good practices for detecting inter-regional linear functional connectivity from EEG. NeuroImage 277, 120218. https://doi.org/10.1016/j.neuroimage.2023.120218

Penny, W.D., Stephan, K.E., Mechelli, A., Friston, K.J., 2004. Comparing dynamic causal models. NeuroImage 22, 1157–1172. https://doi.org/10.1016/j.neuroimage.2004.03.026

Rissman, J., Gazzaley, A., D’Esposito, M., 2004. Measuring functional connectivity during distinct stages of a cognitive task. NeuroImage 23, 752–763. https://doi.org/10.1016/j.neuroimage.2004.06.035

Robinson, E.C., Garcia, K., Glasser, M.F., Chen, Z., Coalson, T.S., Makropoulos, A., Bozek, J., Wright, R., Schuh, A., Webster, M., Hutter, J., Price, A., Cordero Grande, L., Hughes, E., Tusor, N., Bayly, P.V., Van Essen, D.C., Smith, S.M., Edwards, A.D., Hajnal, J., Jenkinson, M., Glocker, B., Rueckert, D., 2018. Multimodal surface matching with higher-order smoothness constraints. NeuroImage 167, 453–465. https://doi.org/10.1016/j.neuroimage.2017.10.037

Robinson, E.C., Jbabdi, S., Glasser, M.F., Andersson, J., Burgess, G.C., Harms, M.P., Smith, S.M., Van Essen, D.C., Jenkinson, M., 2014. MSM: A new flexible framework for Multimodal Surface Matching. NeuroImage 100, 414–426. https://doi.org/10.1016/j.neuroimage.2014.05.069

Ryali, S., Supekar, K., Chen, T., Menon, V., 2011. Multivariate dynamical systems models for estimating causal interactions in fMRI. NeuroImage 54, 807–823. https://doi.org/10.1016/j.neuroimage.2010.09.052

Seth, A.K., Barrett, A.B., Barnett, L., 2015. Granger Causality Analysis in Neuroscience and Neuroimaging. J. Neurosci. 35, 3293–3297. https://doi.org/10.1523/JNEUROSCI.4399-14.2015

Sheikhattar, A., Miran, S., Liu, J., Fritz, J.B., Shamma, S.A., Kanold, P.O., Babadi, B., 2018. Extracting neuronal functional network dynamics via adaptive Granger causality

analysis. Proc. Natl. Acad. Sci. 115, E3869–E3878. https://doi.org/10.1073/pnas.1718154115

Smith, S.M., Miller, K.L., Salimi-Khorshidi, G., Webster, M., Beckmann, C.F., Nichols, T.E., Ramsey, J.D., Woolrich, M.W., 2011. Network modelling methods for FMRI. NeuroImage 54, 875–891. https://doi.org/10.1016/j.neuroimage.2010.08.063

Soleimani, B., Das, P., Dushyanthi Karunathilake, I.M., Kuchinsky, S.E., Simon, J.Z., Babadi, B., 2022. NLGC: Network localized Granger causality with application to MEG directional functional connectivity analysis. NeuroImage 260, 119496. https://doi.org/10.1016/j.neuroimage.2022.119496

Vanderwal, T., Eilbott, J., Finn, E.S., Craddock, R.C., Turnbull, A., Castellanos, F.X., 2017. Individual differences in functional connectivity during naturalistic viewing conditions. NeuroImage 157, 521–530. https://doi.org/10.1016/j.neuroimage.2017.06.027

Vanderwal, T., Kelly, C., Eilbott, J., Mayes, L.C., Castellanos, F.X., 2015. Inscapes : A movie paradigm to improve compliance in functional magnetic resonance imaging. NeuroImage 122, 222–232. https://doi.org/10.1016/j.neuroimage.2015.07.069

Wang, X.-J., 2020. Macroscopic gradients of synaptic excitation and inhibition in the neocortex. Nat. Rev. Neurosci. 21, 169–178. https://doi.org/10.1038/s41583-020-0262-x